Probing Quantum Dynamical Couple Correlations with Time-Domain Interferometry

Salvatore Castrignano and Jörg Evers
Max-Planck-Institut für Kernphysik, Saupfercheckweg 1, 69117 Heidelberg, Germany

(Received 23 May 2018; published 16 January 2019)

Time-domain interferometry (TDI) is a promising method to characterize spatial and temporal correlations at x-ray energies, via the so-called intermediate scattering function and the related dynamical couple correlations. However, so far, it has only been analyzed for classical target systems. Here, we provide a quantum analysis, and suggest a scheme that allows us to access quantum dynamical correlations. We further show how TDI can be used to exclude classical models for the target dynamics, and illustrate our results using a single particle in a double well potential.

DOI: 10.1103/PhysRevLett.122.025301

Introduction.—Spatial and temporal correlations among particles are key to the exploration of complex many-body phenomena. Scattering experiments provide access to the scattering function $S(\mathbf{p},\omega)$ that is proportional to the cross section for scattering with energy transfer $\hbar\omega$ and momentum transfer $\hbar\mathbf{p}$ [1]. It characterizes the evolution of correlations on timescales $\sim 1/\omega$ and length scales $\sim 1/|\mathbf{p}|$. In practice, knowledge of the correlations over a broad range of time and momentum transfer scales is desirable, and various scattering techniques such as x-ray [2,3] and neutron [4] scattering can be used to access complementary energy and momentum transfer scales. Similarly, depending on the properties of the scatterer, it can be favorable to characterize correlations directly in the time domain, via the intermediate scattering function (ISF)

$$S(\mathbf{p},t_1,t_2)=\int_V G(\mathbf{r},t_1,t_2)e^{i\mathbf{p}\cdot\mathbf{r}}d^3r, \tag{1}$$

with the dynamical couple-correlation function (DCF)

$$G(\mathbf{r},t_1,t_2)=\int_V \mathrm{Tr}[\mu\hat{\rho}(\mathbf{r}',t_1)\hat{\rho}(\mathbf{r}'+\mathbf{r},t_2)]d^3r'. \tag{2}$$

Here, the system described by the density matrix μ covers the volume V, and $\hat{\rho}(\mathbf{r},t)$ is the particle-density operator. The DCF quantifies the spatial and temporal correlations between particles at $(\mathbf{r},t_1)$ and $(\mathbf{r}'+\mathbf{r},t_2)$.

A particular technique to access the ISF is the so-called time-domain interferometry (TDI) [5–11] (see Fig. 1 for the extended scheme used here). It has recently been suggested as a promising candidate for x-ray free electron laser experiments (see page 84 of Ref. [2]; note that the general feasibility of free-electron-laser experiments with Mössbauer nuclei has already been demonstrated in a different setting [12]). TDI allows one to measure ISF over much longer times than competing techniques, and it is essentially background-free even for intense x-ray pulses. TDI uses filter foils containing long-lived Mössbauer isotopes, which are placed in front of and behind the actual target. The incident x-ray frequency is chosen in resonance with the Mössbauer nuclear transition. The first foil (which pictorially can be thought of as a "split unit") induces two possible scattering channels for the incoming pulse. The first prompt channel comprises photons which did not interact with the nuclei. The photons in the second channel are delayed in time, due to the interaction with the long-lived nuclear transition. As a consequence, the photons in the two channels probe the target at different times t_1, t_2. After the interaction, the second Mössbauer foil ("overlap unit") again splits each of the two channels into a prompt and a delayed contribution. This "overlap operation" creates scattering channels to the detected signal, which were either delayed in the split unit or in the overlap unit, but not in both, and thus reach the detector at the same time. For these, it is not possible to distinguish if the interaction with the target took place at time t_1 or t_2, and the interference of these two pathways leads to temporal modulations of the detection signal, which in turn provide access to the ISF. Depending on the chosen Mössbauer species, different momentum and energy transfer ranges can be accessed [11]. Recently, also a modified scheme using Mössbauer foils with two resonances has been suggested [13].

So far, TDI has been analyzed and demonstrated experimentally [5,10,11,13,15,16] for targets which can be described by classical mechanics [17]. However, quantum effects change the DCF [1,18], and such quantum corrections have been theoretically studied [19–22] and observed in quantum liquids [23,24] or in surface diffusion [25]. In thermal equilibrium, quantum effects are usually considered to be restricted to relatively short times of order $\hbar/(k_B T)$ [22]. One obvious solution is to lower the temperature, which is taken to the extreme in cold-gas implementations of solid-state dynamics [26,27], where quantum effects were observed in the response functions using inelastic light scattering [28]. But more importantly,

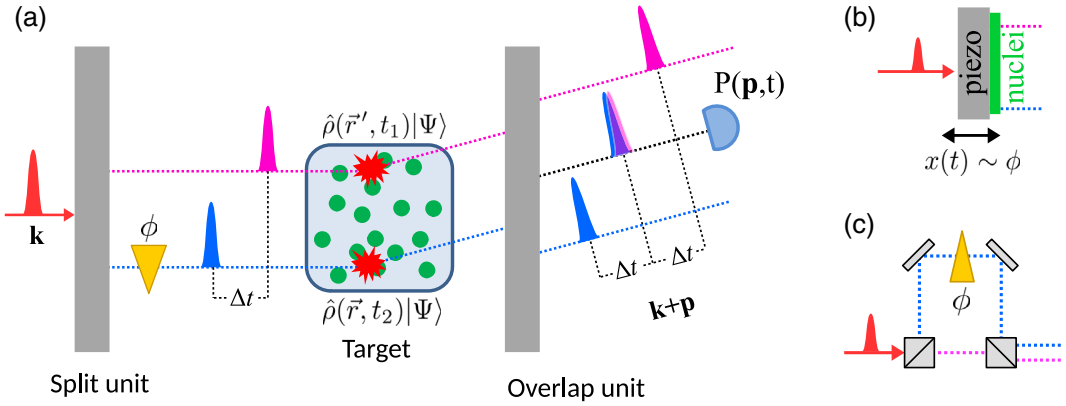

FIG. 1. (a) Schematic setup. The incoming wave packet propagating along $\mathbf{k}$ (red) is separated into two parts with a mutual delay by a split unit. The advanced (violet) component is quasielastically scattered by the target at time t_1, while the delayed one (blue) scatters at t_2. Subsequently, the light scattered in direction $\mathbf{k}+\mathbf{p}$ passes an overlap unit, which acts identical to the split unit. The central component of the outgoing signal contains two indistinguishable contributions, arising from photons which scattered at time t_1 or t_2, respectively. In our scheme, a phase shifter ϕ controls the interference of these two contributions in the measured intensity of the scattered light, and thus enables one to recover the quantum dynamical couple correlation function of the target. (b) If the split and overlap units are realized using Mössbauer filter foils, then the required phase control is possible using mechanical displacements of the split foil as demonstrated in Ref. [14]. (c) A generic implementation of the phase control is a split-and-delay line, with a phase plate in one of the two arms.

a central research goal of modern x-ray sources is the study of strongly correlated and quantum materials, in and out of equilibrium. Their features largely depend on quantum phenomena (see, e.g., Refs. [29–31]), and they exhibit correlations over a broad range of temporal and spatial scales, in particular, out of equilibrium. In this regard, the nanosecond to millisecond scale is considered very interesting, but hard to access experimentally [32,33]. This raises the question of whether time-domain techniques can be used to explore correlations in targets that require a quantum mechanical treatment, this implying a modification of their DCF and ISF by the above mentioned quantum corrections.

Here we provide a quantum mechanical analysis of TDI, and suggest a scheme which allows one to measure the ISF both for quantum and classical targets. In our scheme, the full ISF is accessed by controlling the interference between the different scattering channels via their relative phase. DCF and ISF have different properties for classical and quantum targets and we show how TDI can be used to exclude classical models for the targets. Finally, we illustrate our main results with a minimal model composed of a single particle hopping between two sites.

Properties of DCF and ISF.—We start with symmetry properties of DCF and ISF, which will enable us to distinguish quantum mechanical targets from classical ones. As already noted by van Hove himself in Refs. [1,18], for quantum systems (subscript qu), the DCF is in general a complex-valued function due to the noncommutativity of particle-density operators at different times. It directly follows from definition (2) that

$$G_{\mathrm{qu}}(\mathbf{r}, t_1, t_2)^* = G_{\mathrm{qu}}(-\mathbf{r}, t_2, t_1), \tag{3}$$

$$S_{\mathrm{qu}}(\mathbf{p}, t_1, t_2)^* = S_{\mathrm{qu}}(\mathbf{p}, t_2, t_1). \tag{4}$$

If the system instead is described by a classical model (subscript cl), the density of particles is a real valued function and the quantum mechanical trace is replaced by a statistical ensemble average in Eq. (2). As a consequence, the classical DCF is a real-valued function, giving rise to a different behavior of the ISF under complex conjugation,

$$S_{\mathrm{cl}}(\mathbf{p}, t_1, t_2)^* = S_{\mathrm{cl}}(-\mathbf{p}, t_1, t_2). \tag{5}$$

Note that not only the sign of $\mathbf{p}$ is changed as compared to the quantum case Eq. (4), but also the order of the time arguments t_1, t_2.

Quantum theory of TDI.—We now turn to the analysis of TDI in the case of a quantum target (see Fig. 1). In addition to the original TDI proposal, we assume that the relative phase ϕ between the scattering channels can be controlled. As we will show below, this enables control of the interference between the different scattering channels, and thereby provides access to the full ISF. For Mössbauer foils, the required phase control is possible with sub-Ångstrom precision on a nanosecond scale using mechanical displacements of the split foil, as demonstrated in Ref. [14] [see Fig. 1(b)]. Related precise control of mechanical motion has also been demonstrated in Ref. [34]. In order to simplify the discussion, we consider a setup in which the split and the overlap units separate incoming pulses into two identical copies with mutual delay Δt. One possible realization for this is a split-and-delay line with a phase plate, see Fig. 1(c). Behind the overlap unit, the signal is temporally separated into three pulses. The leading (trailing) pulse comprises those photons which were delayed in none (both) of the split

and overlap units, and which interacted at time t_1 (t_2) with the target. In contrast, the central pulse contains photons which were either delayed in the split unit or in the overlap unit, but not in both. It is therefore not possible to distinguish if the interaction with the target took place at time t_1 or t_2. In the following, we will concentrate on this part. Note that the corresponding quantum analysis of the original setup with Mössbauer foils is given in the Supplemental Material [35].

We proceed by calculating the probability amplitude that a photon from the central pulse is registered by a detector placed at position $\mathbf{R}$ at time t, by summing up the detection amplitudes for the two indistinguishable scattering pathways. These evaluate to ($j \in \{1,2\}$, see Supplemental Material [35] for details)

$$\frac{e^{i\omega_0(R/c-t)}}{R} e^{i\phi_j} f(t) \int_V d^3r e^{-i\mathbf{p}\cdot\mathbf{r}} \hat{\rho}(\mathbf{r}, t_j)|\psi\rangle. \tag{6}$$

As expected, the amplitudes are spherical wave packets with carrier frequency and envelope $f(t)$ identical to those of the incoming photon. The amplitudes depend on the target's density operator at the scattering times and on the initial state of the target $|\psi\rangle$. Here, $\mathbf{p}$ is the exchanged momentum between the photon and the target. The signal recorded by the detector will be proportional to the probability of detecting the photon, which in turn is

$$P(\mathbf{p}, t) \propto f(t)^2 \Bigg(\sum_{j=1,2} S_{qu}(\mathbf{p}, t_j, t_j) + 2\{\cos[\phi] S^R_{qu}(\mathbf{p}, t_1, t_2) - \sin[\phi] S^I_{qu}(\mathbf{p}, t_1, t_2)\} \Bigg), \tag{7}$$

where $\phi = \phi_2 - \phi_1$ is the phase difference between the two scattering pathways. Here and in the following, a superscript R [I] denotes the real [imaginary] part, such that $S_{\mathrm{qu}} = S^R_{\mathrm{qu}} + iS^I_{\mathrm{qu}}$. Note that Eq. (7) applies to targets initially in a pure quantum state. Otherwise, it has to be averaged over all possible initial states.

As our first main result, we find from Eq. (7) that control over the relative phase ϕ and the delay Δt enables one to individually access the real and the imaginary parts of the ISF as a function of momentum transfer $\mathbf{p}$ and time t, as desired.

Next, in order to extract information about the quantum or classical nature of the target, we consider the sum I^+ and the difference I^- of the intensities at two opposite exchanged momenta $\pm\mathbf{p}$. Using Eq. (7),

$$I^{\pm}_{\mathrm{qu}}(\phi, t) \propto f(t)^2 \Bigg(\sum_{j=1,2} [S_{\mathrm{qu}}(\mathbf{p}, t_j, t_j) \pm S_{\mathrm{qu}}(-\mathbf{p}, t_j, t_j)] + 2\{\cos[\phi][S^R_{\mathrm{qu}}(\mathbf{p}, t_1, t_2) \pm S^R_{\mathrm{qu}}(-\mathbf{p}, t_1, t_2)] - \sin[\phi][S^I_{\mathrm{qu}}(\mathbf{p}, t_1, t_2) \pm S^I_{\mathrm{qu}}(-\mathbf{p}, t_1, t_2)]\} \Bigg). \tag{8}$$

If a classical model for the target is assumed, such that the ISF satisfies the symmetry Eq. (5), then Eq. (8) simplifies to

$$I^+_{\mathrm{cl}}(\phi, t) \propto f(t)^2 \Bigg(\sum_{j=1,2} S(\mathbf{p}, t_j, t_j) + 2\cos[\phi] S^R(\mathbf{p}, t_1, t_2) \Bigg), \tag{9}$$

$$I^-_{\mathrm{cl}}(\phi, t) \propto -2 f(t)^2 \sin[\phi] S^I(\mathbf{p}, t_1, t_2). \tag{10}$$

Thus, recording $I^{\pm}$ for different values of ϕ enables one to distinguish quantum or classical symmetries of the target. If, e.g., I^- does not vanish at $\phi = n\pi$, then the classical relation Eq. (10) is ruled out. It follows that the ISF of the target has no inversion symmetry, such that the DCF is a complex valued function and a quantum model for the target is needed. In the opposite case, DCF is real valued. Then, it may still be possible to violate Eq. (9) to exclude a classical model. However, it is important to note that a real DCF alone does not imply a classical target. Rather, also quantum targets may exhibit real valued DCF for particular parameter choices. This fact is explicitly shown for a concrete system in the next section.

Model.—In the final part, we illustrate our results with a single particle in a double well potential. The DCF and ISF for this simple model can be calculated exactly, explicitly showing that a nonvanishing imaginary part of the DCF can be attributed to the existence of quantum coherences. These coherences arise if the particle is in a coherent superposition of position eigenstates. However, the reverse is not true, since we find particular superposition states for which the DCF is real valued.

We denote the two wells by L and R, and the particle dynamics is governed by the Hamiltonian

$$H = -\hbar \frac{\Omega}{2} (|L\rangle\langle R| + |R\rangle\langle L|). \tag{11}$$

A generic state of the particle at time t in the $|L\rangle$, $|R\rangle$ representation is given by the density matrix

$$\mu(t) = \begin{pmatrix} P_L(t) & \Gamma(t) \\ \Gamma(t)^* & P_R(t) \end{pmatrix}, \tag{12}$$

where $P_L(t)[P_R(t)]$ are the probabilities of finding the particle at time t at position $L[R]$ which satisfy the condition $P_L(t) + P_R(t) = 1$, while $\Gamma(t)$ is the coherence coefficient. The DCF calculated for the state (12) is

$$G_{\mathrm{qu}}(\mathbf{d}, t_1, t_2) = \mathcal{S}^2 P_L(t_1) + \frac{i}{2} \mathcal{S}' \Gamma(t_1)^*, \tag{13}$$

$$G_{\mathrm{qu}}(-\mathbf{d}, t_1, t_2) = \mathcal{S}^2 P_R(t_1) + \frac{i}{2} \mathcal{S}' \Gamma(t_1), \tag{14}$$

$$G_{\mathrm{qu}}(0,t_1,t_2) = \mathcal{C} - i\mathcal{S}'\Gamma^R(t_1), \tag{15}$$

where $\mathcal{S} = \sin[\Omega\Delta t/2]$, $\mathcal{C} = \cos[\Omega\Delta t/2]$, $\mathcal{S}' = \sin[\Omega\Delta t]$, $\Delta t = t_2 - t_1$, and $\Gamma^R(t_1)$ indicates the real part of $\Gamma(t_1)$. Expressions (13)–(15) are complex valued if $\Gamma^R(t_1)$ is nonzero, that is when the particle is in a coherent superposition of $|L\rangle$ and $|R\rangle$. On the contrary, a purely imaginary $\Gamma(t_1)$ gives a real DCF even though the state is in a quantum superposition. Thus, we find that a real valued DCF alone does not imply classical behavior.

The ISF corresponding to (13)–(15) is

$$\begin{aligned} S_{\mathrm{qu}}(\mathbf{p},t_1,t_2) = {} & \mathcal{S}^2\cos[\mathbf{p}\cdot\mathbf{d}] + \mathcal{C}^2 \\ & + i\Big\{[P_L(t_1) - P_R(t_1)]\mathcal{S}^2\sin[\mathbf{p}\cdot\mathbf{d}] \\ & + \frac{\mathcal{S}'}{2}[\Gamma^I(t_1)\sin[\mathbf{p}\cdot\mathbf{d}] \\ & + \Gamma^R(t_1)(\cos[\mathbf{p}\cdot\mathbf{d}] - 2)]\Big\}, \end{aligned} \tag{16}$$

which evidently satisfies the identity (5) only if $\Gamma^R(t_1) = 0$, consistently with the results for the DCF. It turns out that Γ^R is a constant of motion under the action of Hamiltonian Eq. (11). This allows us to relate the results better to an actual experimental implementation, in which it may only be possible to control the delay Δt, but not t_1 itself. Averaging over t_1, we find

$$\bar{G}_{\mathrm{qu}}(\pm\mathbf{d},\Delta t) = \frac{1}{2}\mathcal{S} + \frac{i}{2}\mathcal{S}'\Gamma^R, \tag{17}$$

$$\bar{G}_{\mathrm{qu}}(0,\Delta t) = \mathcal{C} - i\mathcal{S}'\Gamma^R, \tag{18}$$

$$\begin{aligned} \bar{S}_{\mathrm{qu}}(\mathbf{p},\Delta t) = {} & \mathcal{S}^2\cos[\mathbf{p}\cdot\mathbf{d}] + \mathcal{C}^2 \\ & + \frac{i}{2}(\cos[\mathbf{p}\cdot\mathbf{d}] - 2)\mathcal{S}'\Gamma^R. \end{aligned} \tag{19}$$

As before, the complex nature of the DCF is linked to Γ^R. From Eq. (10), we further find $\bar{I}^- = 0$, such that a classical model cannot be excluded. But $\bar{I}^+$ has a contribution proportional to $\Gamma^R\sin\phi$, which is at odds with Eq. (9) if $\Gamma^R \neq 0$, such that then a classical model can be excluded.

Summary and discussion.—DCF and ISF have different properties for quantum and classical systems. The noncommutativity of particle-density operators at different times in general leads to imaginary contributions to the DCF for quantum systems, and DCF and ISF have different symmetry properties under complex conjugation for classical and quantum systems. Using the quantum mechanical analysis presented here, we have shown that time-domain techniques can be used to measure the complex-valued ISF. Moreover, the comparison of the ISF at two opposite values of the exchanged momentum $\mathbf{p}$ in the form Eq. (8) provides access to the symmetry properties of the system's ISF, and gives a handle to exclude classical models for the target. Throughout the analysis, we used a simplified model for the split and overlap units, but our results carry over to the case of Mössbauer filter foils (see Supplemental Material [35]), for which the required relative-phase control is possible with the necessary precision [14,34].

While quantum corrections to the DCF already appear in thermal equilibrium, a suitable preparation of the sample is expected to induce quantum effects, and to render them more accessible, e.g., by reducing detrimental averagings in the measurement. Pulsed laser systems synchronized to the x rays are under development at most x-ray facilities, and have also already been demonstrated with Mössbauer nuclei [36]. Our TDI scheme is not restricted to the x-ray domain, but could also be used to explore correlations on other timescales and length scales, such as cold-atom implementations of solid state dynamics [28]. This requires the availability of suitable split and overlap units, and a system whose internal dynamics has no resonance in the spectrum of the probing photon pulse, so that only quasielastic scattering of the photon is relevant. The analysis of our simple double-well model could serve as a starting point for the investigation of related phenomena in more realistic settings. For example, cold atoms trapped in atomic lattices serve as quantum simulators for complex solid state phenomena, structured periodic potentials appear on surfaces of materials, and certain complex materials may intrinsically offer various quantum states placed in a periodic potential landscape. Few-particle systems in single- or double-well potentials have also been studied directly [37]. Finally, we note that the appearance of imaginary parts in such quantities poses practical and interpretative problems [38–40], which could be explored experimentally using TDI techniques.

This work is part of and supported by the DFG Collaborative Research Centre "SFB 1225 (ISOQUANT)."

[1] L. Van Hove, Correlations in space and time and Born approximation scattering in systems of interacting particles, Phys. Rev. **95**, 249 (1954).

[2] L. Heyderman, C. Milne, P. Thibault, K. Ballmer, and U. Staub, Ultrafast Phenomena at the Nanoscale: Science opportunities at the SwissFEL X-ray Laser, Paul Scherrer Institut, Technical Report 09-10, 2009.

[3] R. Abela, P. Beaud, J. A. van Bokhoven, M. Chergui, T. Feurer, J. Haase, G. Ingold, S. L. Johnson, G. Knopp, H. Lemke, C. J. Milne, B. Pedrini, P. Radi, G. Schertler, J. Standfuss, U. Staub, and L. Patthey, Perspective: Opportunities for ultrafast science at SwissFEL, Struct. Dyn. **4**, 061602 (2018).

[4] S. W. Lovesey, *Theory of Neutron Scattering from Condensed Matter–Volume I: Nuclear Scattering* (Oxford University Press, Oxford, 1986).

[5] A. Q. R. Baron, H. Franz, A. Meyer, R. Rüffer, A. I. Chumakov, E. Burkel, and W. Petry, Quasielastic Scattering of Synchrotron Radiation by Time Domain Interferometry, Phys. Rev. Lett. **79**, 2823 (1997).

[6] G. V. Smirnov, V. G. Kohn, and W. Petry, Dynamics of electron density in a medium revealed by Mössbauer time-domain interferometry, Phys. Rev. B **63**, 144303 (2001).

[7] G. V. Smirnov, U. van Bürck, H. Franz, T. Asthalter, O. Leupold, E. Schreier, and W. Petry, Nuclear γ resonance time-domain interferometry: Quantum beat and radiative coupling regimes compared in revealing quasielastic scattering, Phys. Rev. B **73**, 184126 (2006).

[8] M. Saito, M. Seto, S. Kitao, Y. Kobayashi, M. Kurokuzu, and Y. Yoda, Time-domain interferometry experiments using multi-line nuclear absorbers, Hyperfine Interact. **206**, 87 (2012).

[9] M. Saito, R. Masuda, Y. Yoda, and M. Seto, Synchrotron radiation-based quasi-elastic scattering using time-domain interferometry with multi-line gamma rays, Nat. Sci. Rep. Ochanomizu Univ. **7**, 12558 (2017).

[10] M. Kaisermayr, B. Sepiol, H. Thiess, G. Vogl, E. E. Alp, and W. Sturhahn, Time-domain interferometry using synchrotron radiation applied to diffusion in ordered alloys, Eur. Phys. J. B **20**, 335 (2001).

[11] M. Saito, M. Seto, S. Kitao, Y. Kobayashi, S. Higashitaniguchi, M. Kurokuzu, M. Sugiyama, and Y. Yoda, Development of ^{151}Eu time-domain interferometry and its application for the study of slow dynamics in ionic liquids, Appl. Phys. Express **2**, 026502 (2009).

[12] A. I. Chumakov, A. Q. R. Baron, I. Sergueev, C. Strohm, O. Leupold, Y. Shvyd'ko, G. V. Smirnov, R. Rüffer, Y. Inubushi, M. Yabashi, K. Tono, T. Kudo, and T. Ishikawa, Superradiance of an ensemble of nuclei excited by a free electron laser, Nat. Phys. **14**, 261 (2018).

[13] F. Caporaletti, A. I. Chumakov, R. Rüffer, and G. Monaco, A new experimental scheme for nuclear γ-resonance time-domain interferometry, Rev. Sci. Instrum. **88**, 105114 (2017).

[14] K. P. Heeg, A. Kaldun, C. Strohm, P. Reiser, C. Ott, R. Subramanian, D. Lentrodt, J. Haber, H.-C. Wille, S. Goerttler, R. Rüffer, C. H. Keitel, R. Röhlsberger, T. Pfeifer, and J. Evers, Spectral narrowing of x-ray pulses for precision spectroscopy with nuclear resonances, Science **357**, 375 (2017).

[15] M. Saito, S. Kitao, Y. Kobayashi, M. Kurokuzu, Y. Yoda, and M. Seto, Slow Processes in Supercooled *o*-terphenyl: Relaxation and Decoupling, Phys. Rev. Lett. **109**, 115705 (2012).

[16] M. Saito, A. Battistoni, S. Kitao, Y. Kobayashi, M. Kurokuzu, Y. Yoda, and M. Seto, Slow dynamics of supercooled liquid revealed by Rayleigh scattering of Mössbauer radiation method in time domain, Hyperfine Interact. **226**, 629 (2014).

[17] J. P. Hansen and I. R. McDonald, *Theory of Simple Liquids* (Academic Press, New York, 2013).

[18] L. Van Hove, A remark on the time-dependent pair distribution, Physica **24**, 404 (1958).

[19] G. I. Watson, Neutron compton scattering, J. Phys. Condens. Matter **8**, 5955 (1996).

[20] F. Barocchi, M. Moraldi, and M. Zoppi, "Almost classical" many-body systems: The quantum-mechanical corrections to the moments of a general spectrum, Phys. Rev. A **26**, 2168 (1982).

[21] V. F. Sears, Neutron scattering in almost-classical liquids, Phys. Rev. A **31**, 2525 (1985).

[22] P. Schofield, Space-Time Correlation Function Formalism for Slow Neutron Scattering, Phys. Rev. Lett. **4**, 239 (1960).

[23] A. Cunsolo, D. Colognesi, M. Sampoli, R. Senesi, and R. Verbeni, Signatures of quantum behavior in the microscopic dynamics of liquid hydrogen and deuterium, J. Chem. Phys. **123**, 114509 (2005).

[24] A. Cunsolo, G. Monaco, M. Nardone, G. Pratesi, and R. Verbeni, Transition from the collective to the single-particle regimes in a quantum fluid, Phys. Rev. B **67**, 024507 (2003).

[25] A. P. Jardine, G. Alexandrowicz, H. Hedgeland, W. Allison, and J. Ellis, Studying the microscopic nature of diffusion with helium-3 spin-echo, Phys. Chem. Chem. Phys. **11**, 3355 (2009).

[26] C. Gross and I. Bloch, Quantum simulations with ultracold atoms in optical lattices, Science **357**, 995 (2017).

[27] I. M. Georgescu, S. Ashhab, and F. Nori, Quantum simulation, Rev. Mod. Phys. **86**, 153 (2014).

[28] R. Landig, F. Brennecke, R. Mottl, T. Donner, and T. Esslinger, Measuring the dynamic structure factor of a quantum gas undergoing a structural phase transition, Nat. Commun. **6**, 7046 (2015).

[29] B. Keimer and J. E. Moore, The physics of quantum materials, Nat. Phys. **13**, 1045 (2017).

[30] E. Dagotto, Complexity in strongly correlated electronic systems, Science **309**, 257 (2005).

[31] J. Quintanilla and C. Hooley, The strong-correlations puzzle, Phys. World **22**, 32 (2009).

[32] C. G. Schroer, I. Agapov, W. Brefeld, R. Brinkmann, Y.-C. Chae, H.-C. Chao, M. Eriksson, J. Keil, X. N. Gavaldà, R. Röhlsberger, O. H. Seeck, M. Sprung, M. Tischer, R. Wanzenberg, and E. Weckert, PETRA IV: The ultralow-emittance source project at DESY, J. Synchrotron Radiat. **25**, 1277 (2018).

[33] M. H. Seaberg, B. Holladay, J. C. T. Lee, M. Sikorski, A. H. Reid, S. A. Montoya, G. L. Dakovski, J. D. Koralek, G. Coslovich, S. Moeller, W. F. Schlotter, R. Streubel, S. D. Kevan, P. Fischer, E. E. Fullerton, J. L. Turner, F.-J. Decker, S. K. Sinha, S. Roy, and J. J. Turner, Nanosecond X-Ray Photon Correlation Spectroscopy on Magnetic Skyrmions, Phys. Rev. Lett. **119**, 067403 (2017).

[34] F. Vagizov, V. Antonov, Y. V. Radeonychev, R. N. Shakhmuratov, and O. Kocharovskaya, Coherent control of the waveforms of recoilless γ-ray photons, Nature (London) **508**, 80 (2014).

[35] See Supplemental Material at http://link.aps.org/supplemental/10.1103/PhysRevLett.122.025301 for probing quantum dynamical couple correlations with time-domain interferometry.

[36] S. Sakshath, K. Jenni, L. Scherthan, P. Würtz, M. Herlitschke, I. Sergeev, C. Strohm, H.-C. Wille, R. Röhlsberger, J. A. Wolny, and V. Schünemann, Optical pump—nuclear resonance probe experiments on spin crossover complexes, Hyperfine Interact. **238**, 89 (2017).

[37] S. Murmann, A. Bergschneider, V. M. Klinkhamer, G. Zürn, T. Lompe, and S. Jochim, Two Fermions in a Double Well: Exploring a Fundamental Building Block of the Hubbard Model, Phys. Rev. Lett. **114**, 080402 (2015).

[38] L. E. Ballentine, *Fundamental Problems in Quantum Physics* (Springer, New York, 1995), pp. 15–28.

[39] H. Margenau and R. N. Hill, Correlation between measurements in quantum theory, Prog. Theor. Phys. **26**, 722 (1961).

[40] P. Uhrich, S. Castrignano, H. Uys, and M. Kastner, Noninvasive measurement of dynamic correlation functions, Phys. Rev. A **96**, 022127 (2017).